The Low-Redshift Intergalactic Medium as Seen in Archival Legacy Hubble/STIS and FUSE Data

Evan M. Tilton[1], Charles W. Danforth[1], J. Michael Shull[1], Teresa L. Ross[2]

[1]CASA, University of Colorado at Boulder; [2]Department of Astronomy, New Mexico State University

Submitted to ApJ. Available at arXiv:1204.3623.

Abstract

We present a comprehensive catalog of ultraviolet (HST/STIS and FUSE) absorbers in the low-redshift IGM at z<0.4. The catalog draws from much of the extensive literature on IGM absorption, and it reconciles discrepancies among several previous catalogs through a critical evaluation of all reported absorption features in light of new HST/COS data. We report on 746 H I absorbers down to a rest-frame equivalent width of 12 mA over a maximum redshift path length Δz=5.38. We also confirm 111 O VI absorbers, 29 C IV absorbers, and numerous absorption lines due to other metal ions. We characterize the bivariate distribution of absorbers in redshift and column density as a power law, $\partial^2 N/\partial z/\partial N \propto N^{-\beta}$, where β=2.08±0.12 for O VI and β=1.68±0.03 for H I. Utilizing a more sophisticated accounting technique than past work, the catalog accounts for ~43% of the baryons: 24±2% in the photoionized Lyα forest and 19±2% in the WHIM as traced by O VI. We discuss the large systematic effects of various assumed metallicities and ionization states on these calculations, and we implement recent simulation results (Shull et al. 2012) in our estimates.

Motivation

- Most of the baryon density of the universe resides in the IGM. Roughly one-third of the baryons in the low-z IGM remain undetected observationally.
- At low redshift, roughly 30% of the baryonic matter is in the photoionized Lyman alpha forest, while the rest is in the warm-hot IGM (WHIM), galaxies, clusters, and the circumgalactic medium (CGM).
- The IGM gas phases are best characterized by UV and X-Ray absorption spectroscopy, and much of the past work has focused on FUSE and HST observations.
- With COS, sensitivity to these absorbers is at an all time high. We therefore attempt develop a complete catalog of absorbers in archival HST/STIS and FUSE data that may serve to guide new COS work and obtain new estimates of the absorber distribution at low redshift.

Method

- Search literature for known STIS and FUSE absorbers (H I, O VI, N V, C IV, C III, Si IV, Si III, Fe III, C II, Fe II, Si II, S II, S III, S IV).
- Critically evaluate reported measurements in light of other work and STIS, FUSE, and (if available) COS data to determine a consensus, best estimate interpretation and measurement from the STIS and FUSE data.
- For sightlines without existing absorber lists in the literature, complete new sightline analysis.
- Search all redshift with absorption due to any species for absorption due to a variety of other species.
- Utilize recent IGM simulation results along with new catalog to estimate baryon densities.

Results

- Detections are summarized in the table below.
- Distributions for these ions are shown in Figures 1, 3, and 4. The Doppler b-value distributions for H I and O VI are shown in Figures 2 and 5, respectively.

Summary of IGM Detections and Results

Ion	$\mathcal{N}_{\rm total}$	$\mathcal{N}$	$z_{\rm abs}$	$\Delta z_{\rm max}$	$d\mathcal{N}/dz^{\rm a}$ (> 10 mÅ)	$d\mathcal{N}/dz^{\rm a}$ (> 21 mÅ)	$d\mathcal{N}/dz^{\rm a}$ (> 30 mÅ)	β
(1)	(2)	(3)	(4)	(5)	(6)	(7)	(8)	(9)
O VI	118	111	< 0.40	6.095	$42.0^{+10.7}_{-6.3}$	$27.7^{+3.8}_{-2.9}$	$22.2^{+3.2}_{-2.4}$	2.075 ± 0.119
N V	29	25	< 0.396	5.408	$70.4^{+47.1}_{-24.1}$	$20.6^{+8.2}_{-5.1}$	$9.6^{+5.4}_{-2.7}$	2.001 ± 0.235
C IV	36	29	< 0.116	2.523	$14.3^{+4.5}_{-2.5}$	$14.3^{+4.5}_{-2.5}$	$11.7^{+3.7}_{-2.0}$	1.774 ± 0.157
C III	51	50	< 0.40	5.644	$23.8^{+10.9}_{-4.7}$	$17.3^{+4.7}_{-2.7}$	$14.4^{+3.7}_{-2.2}$	1.859 ± 0.092
Si IV	34	30	< 0.24	4.317	$15.4^{+6.7}_{-3.0}$	$11.8^{+4.0}_{-2.1}$	$9.2^{+3.5}_{-1.8}$	1.729 ± 0.125
Si III	62	57	< 0.40	5.244	$16.6^{+4.1}_{-2.6}$	$10.4^{+2.4}_{-1.5}$	$7.4^{+2.1}_{-1.2}$	1.739 ± 0.102
H I	797	746	< 0.40	5.382	$283.9^{+57.2}_{-32.8}$	$175.2^{+13.0}_{-9.8}$	$144.0^{+6.6}_{-6.0}$	1.680 ± 0.030
Poorly Constrained Ion Species								
Fe III	15	11	< 0.40	5.853	$9.3^{+5.2}_{-2.6}$	$5.4^{+4.2}_{-1.8}$	$3.7^{+3.5}_{-1.4}$	2.216 ± 0.428
C II	18	18	< 0.296	4.900	$9.6^{+5.3}_{-2.2}$	$8.0^{+3.7}_{-1.8}$	$7.5^{+3.5}_{-1.7}$	1.587 ± 0.121
Fe II	5	4	< 0.40	5.913	$11.2^{+13.8}_{-5.0}$	$4.3^{+7.0}_{-2.5}$	$4.3^{+7.0}_{-2.5}$	1.922 ± 1.505
Si II	15	15	< 0.372	5.345	$7.1^{+3.6}_{-1.7}$	$7.1^{+3.6}_{-1.7}$	$6.1^{+3.3}_{-1.5}$	1.568 ± 0.157
S II	3	3	< 0.373	5.352	$10.0^{+13.4}_{-4.8}$	$6.2^{+10.1}_{-3.6}$	$3.1^{+7.1}_{-2.5}$	1.568 ± 0.157
S III[b]	1	1	< 0.40	5.924	...	...	...	...
S IV[b]	0	0	< 0.40	5.889	...	...	...	...
N II[c]	8	8	...	...	...	...	...	...
N III[c]	3	3	...	...	...	...	...	...

[a] Number of absorbers per unit redshift path length, integrated down to the indicated equivalent width.
[b] No statistics are presented for this ion species owing to a lack of detections.
[c] Though several detections of this ion are reported in the catalog, no systematic search was made for this species. As a result, all detections were serendipitous and any statistics derived from those detections may be heavily biased. We therefore refrain from reporting any such statistics but note the detections for completeness.

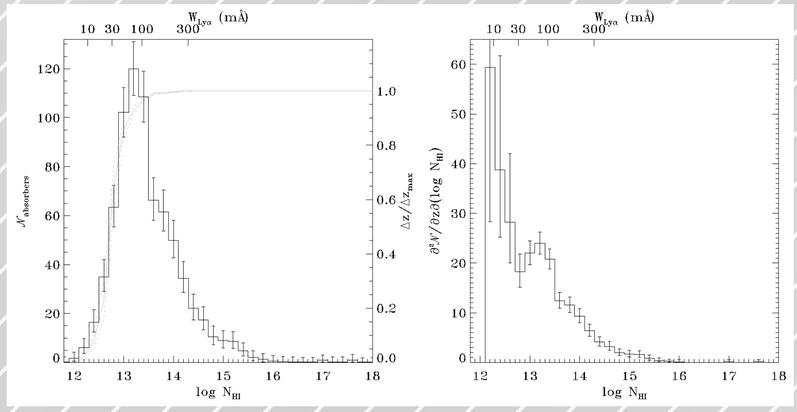

Fig 1. Distributed histograms of detection statistics and $\partial^2 N/\partial z \partial$(logN) vs. logN for H I. The completeness in terms of effective path length, $\Delta z/\Delta z_{\rm max}$, is shown by the gray curve using the right axes. The dashed lines show the one-sigma error on the effective path length.

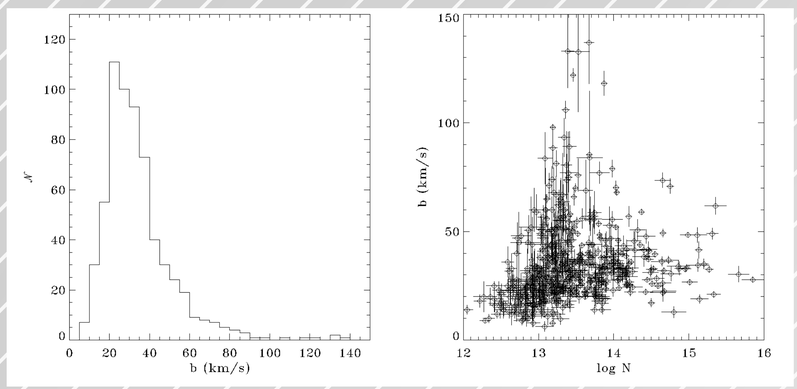

Fig 2. Distribution of H I b-values for absorbers with measurement errors less than 50%. Some absorbers may be blended components, so these b-values are upper limits only. The median is 30 km/s and the standard deviation is 17 km/s.

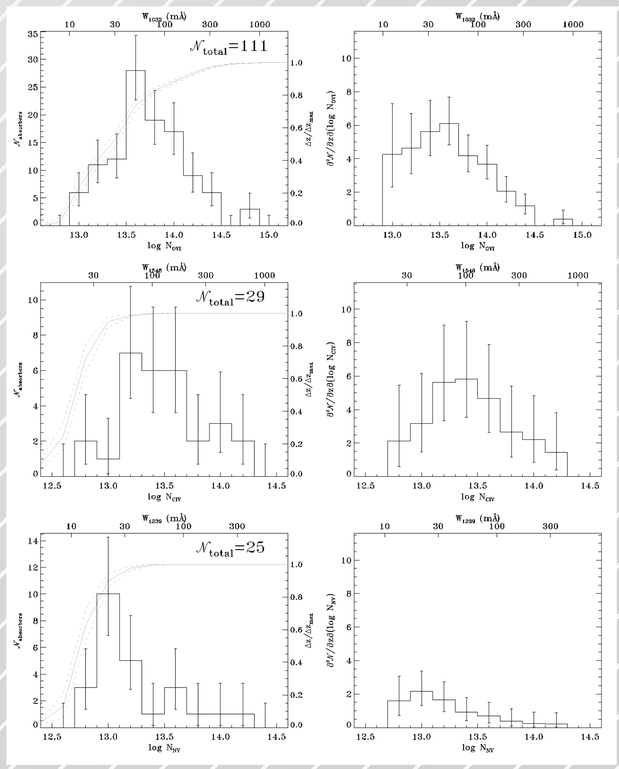

Fig #. Simple histograms of detection statistics and distributed histograms of $\partial^2 N/\partial z \partial$(logN) vs. logN for O VI (top), C IV (middle), and N V (bottom). The completeness in effective path length, $\Delta z/\Delta z_{\rm max}$, is shown by gray curves using right axes. Dashed lines show one-sigma errors on the effective path length.

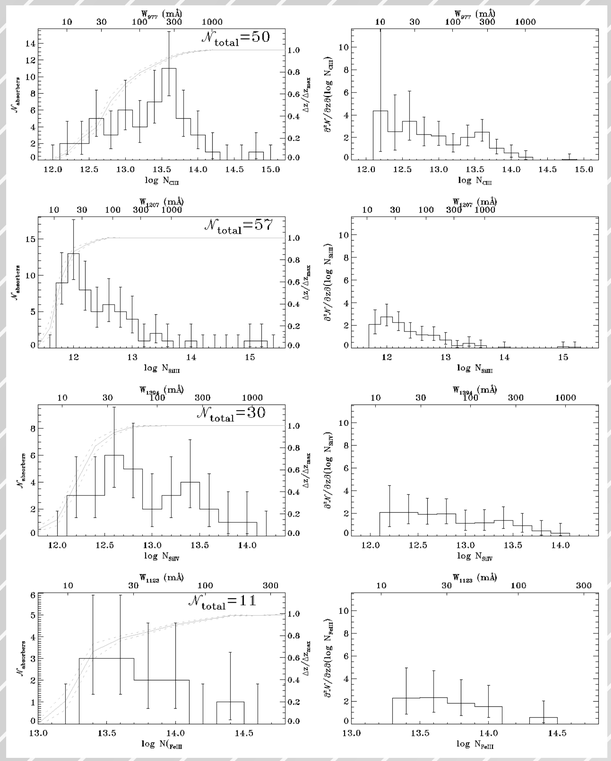

Fig #. Simple histograms of detection statistics and distributed histograms of $\partial^2 N/\partial z \partial$(logN) vs. logN for C III (top), Si III (second row), Si IV (third row) and Fe III (bottom). The completeness in effective path length, $\Delta z/\Delta z_{\rm max}$, is shown by gray curves using the right axes. Dashed lines show one-sigma errors on the effective path length.

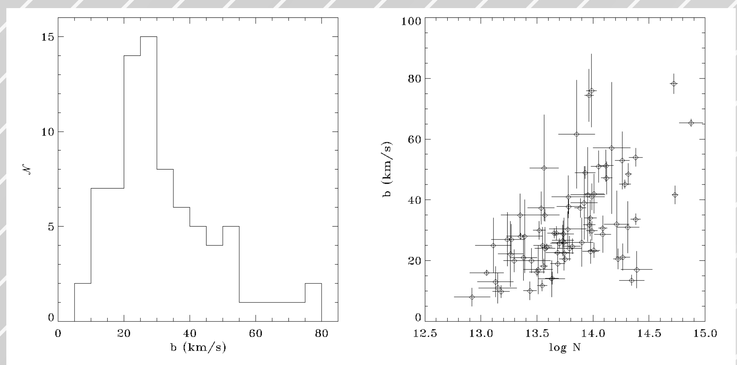

Fig 5. Distibution of b-values for O VI absorbers with measurement errors less than 50%. The median is 28 km/s and the standard deviation is 16 km/s.

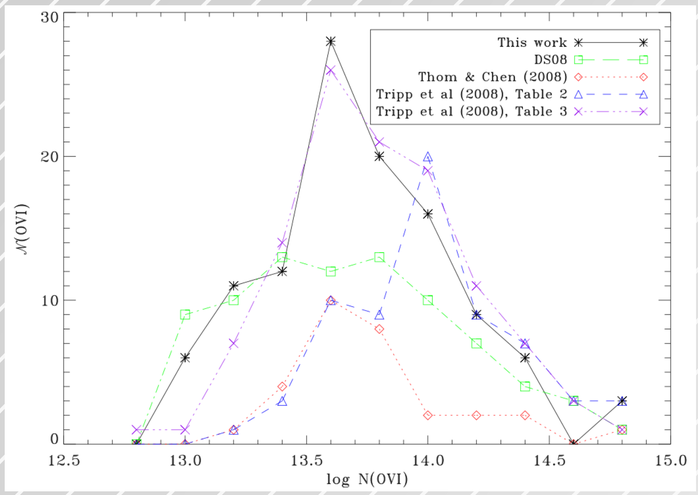

Fig 6. O VI detections from this catalog compared to those of several other catalogs.

- Instead of assuming peak CIE, we also compute Ω using column density dependent fits to results for $f_{\rm ion}(Z/Z_{\rm solar})$ from Shull et al. (2012). This yields higher values: 18.9±2.0% (O VI), 10.1±6.0% (N V), 22.3±3.7% (C IV). These results may be affected by the photoionization scheme used in the simulations, however.
- Overall, the catalog accounts for around 43% of Ω_b. This, however, neglects double counting between the WHIM and the Lyman alpha forest, which likely inflates the estimate to some degree.

Discussion

- This catalog is significantly different from some of the other major low-z IGM catalogs. See Figure 6 for an O VI comparison. Major differences arise from treatment of subcomponents, increased number of sightlines (44), and corrections of previous misidentifications.
- There are hints of turnovers in the O VI, C IV, and N V column-density distributions. It is unclear whether these are significant, as they may be due to sample size, completeness, or inhomogeneity in the catalog. Fitting only the bins beyond the turnover yields steeper slopes (β=2.5 for O VI).
- At high logN, the O VI distribution compares favorably to CIE simulations, but the simulations over-predict the low end compared to the observations.
- All but 4 O VI absorbers are associated with H I absorbers.

Baryon Density

- We calculate the Lyman alpha forest baryon density from the H I catalog using three methods, summarized below. The Shull et al. (2012) method is preferred, as it accounts for the redshift dependence of the photoionizing background and the evolution in space density of absorbers.
- The baryon densities for the metal ions are shown at right. The rightmost two columns correct for abundance (0.1 solar) and ionization fraction assuming peak CIE.

Baryon Content of the Local Lyα Forest

log $N_{\rm HI}$ Range	$\mathcal{N}$	$\Omega_{\rm Ly\alpha}$ [a]	$\Omega_{\rm Ly\alpha}/\Omega_b$ (%) [a]	$\Omega_{\rm Ly\alpha}$ [b]	$\Omega_{\rm Ly\alpha}/\Omega_b$ (%) [b]	$\Omega_{\rm Ly\alpha}$ [c]	$\Omega_{\rm Ly\alpha}/\Omega_b$ (%) [c]
12.0 − 12.5	20	0.0055 ± 0.0043	12.0 ± 9.5	0.0038 ± 0.0041	8.3 ± 9.0	0.0036 ± 0.0041	8.0 ± 8.9
12.5 − 13.5	427	0.0044 ± 0.0010	9.8 ± 2.2	0.0039 ± 0.0008	8.6 ± 1.8	0.0038 ± 0.0008	8.4 ± 1.7
13.5 − 14.5	244	0.0031 ± 0.0003	6.7 ± 0.6	0.0038 ± 0.0003	8.4 ± 0.8	0.0038 ± 0.0003	8.3 ± 0.7
14.5 − 15.5	49	0.0012 ± 0.0002	2.7 ± 0.5	0.0023 ± 0.0004	5.0 ± 1.0	0.0022 ± 0.0004	4.9 ± 0.9
15.5 − 16.5	3	0.0001 ± 0.0001	0.3 ± 0.2	0.0003 ± 0.0002	0.7 ± 0.4	0.0003 ± 0.0002	0.7 ± 0.4
12.5 − 14.5	671	0.0075 ± 0.0010	16.5 ± 2.3	0.0077 ± 0.0009	17.0 ± 1.9	0.0076 ± 0.0008	16.6 ± 1.8
14.5 − 16.5	52	0.0013 ± 0.0002	2.9 ± 0.5	0.0026 ± 0.0005	5.7 ± 1.0	0.0026 ± 0.0005	5.7 ± 1.0
16.5 − 19.0	3	0.0006 ± 0.0004	1.4 ± 0.8	0.0035 ± 0.0022	7.8 ± 4.8	0.0035 ± 0.0021	7.7 ± 4.7
12.5 − 16.5	723	0.0088 ± 0.0011	19.4 ± 2.3	0.0103 ± 0.0010	22.7 ± 2.2	0.0102 ± 0.0010	22.3 ± 2.1
12.5 − 19.0	726	Shull method for log $N_{\rm HI} < 16.5$, Schaye method for log $N_{\rm HI} > 16.5$:				0.0108 ± 0.0010	23.7 ± 2.2

[a] Method of Penton et al. (2000)
[b] Method of Schaye (2001)
[c] Method of Shull et al. (2011)

REFERENCES

Aracil, B., Tripp, T. M., Bowen, D. V., Prochaska, J. X., Chen, H.-W., & Frye, B. L. 2006, MNRAS, 367, 139
Asplund, M., Grevesse, N., Sauval, A. J., & Scott, P. 2009, ARA&A, 47, 481
Bahcall, J. N., & Peebles, P. J. E. 1969, ApJ, 156, L7
Cen, R., & Fang, T. 2006, ApJ, 650, 573
Cen, R., & Ostriker, J. P. 1999, ApJ, 519, L109
Danforth, C. W., Keeney, B. A., Stocke, J. T., Shull, J. M., & Yao, Y. 2010, ApJ, 720, 976
Danforth, C. W., & Shull, J. M. 2005, ApJ, 624, 555
—. 2008, ApJ, 679, 194
Danforth, C. W., Shull, J. M., Rosenberg, J. L., & Stocke, J. T. 2006, ApJ, 640, 716
Danforth, C. W., Stocke, J. T., Keeney, B. A., Penton, S. V., Shull, J. M., Yao, Y., & Green, J. C. 2011, ApJ, 743, 18
Davé, R., et al. 2001, ApJ, 552, 473
Ganguly, R., Masiero, J., Charlton, J. C., & Sembach, K. R. 2003, ApJ, 598, 922
Gehrels, N. 1986, ApJ, 303, 336
Green, J. C., et al. 2012, ApJ, 744, 60
Haardt, F., & Madau, P. 2012, ApJ, 746, 125
Howk, J. C., Ribaudo, J. S., Lehner, N., Prochaska, J. X., & Chen, H.-W. 2009, MNRAS, 396, 1875
Jenkins, E. B., Bowen, D. V., Tripp, T. M., Sembach, K. R., Leighly, K. M., Halpern, J. P., & Lauroesch, J. T. 2003, AJ, 125, 2824
Komatsu, E., et al. 2011, ApJS, 192, 18
Lehner, N., Savage, B. D., Richter, P., Sembach, K. R., Tripp, T. M., & Wakker, B. P. 2007, ApJ, 658, 680
Lehner, N., Savage, B. D., Wakker, B. P., Sembach, K. R., & Tripp, T. M. 2006, ApJS, 164, 1
Moos, H. W., et al. 2000, ApJ, 538, L1
Morton, D. C. 2003, ApJS, 149, 205
Narayanan, A., et al. 2011, ApJ, 730, 15
Oegerle, W. R., et al. 2000, ApJ, 538, L23
Peimbert, M., Luridiana, V., & Peimbert, A. 2007, ApJ, 666, 636
Penton, S. V., Shull, J. M., & Stocke, J. T. 2000, ApJ, 544, 150
Penton, S. V., Stocke, J. T., & Shull, J. M. 2004, ApJS, 152, 29
Prochaska, J. X., Chen, H.-W., Howk, J. C., Weiner, B. J., & Mulchaey, J. 2004, ApJ, 617, 718
Ralchenko, Y., Kramida, A., Reader, J., & NIST ASD Team. 2010, NIST Atomic Spectra Database (version 4.0)
Richter, P., Fang, T., & Bryan, G. L. 2006, A&A, 451, 767
Richter, P., Savage, B. D., Tripp, T. M., & Sembach, K. R. 2004, ApJS, 153, 165
Richter, P., Savage, B. D., Wakker, B. P., Sembach, K. R., & Kalberla, P. M. W. 2001, ApJ, 549, 281
Savage, B. D., Lehner, N., & Narayanan, A. 2011a, ApJ, 743, 180
Savage, B. D., Narayanan, A., Lehner, N., & Wakker, B. P. 2011b, ApJ, 731, 14
Savage, B. D., Sembach, K. R., Tripp, T. M., & Richter, P. 2002, ApJ, 564, 631
Savage, B. D., Wakker, B. P., Fox, A. J., & Sembach, K. R. 2005, ApJ, 619, 863
Schaye, J. 2001, ApJ, 559, 507
Sembach, K. R., Howk, J. C., Savage, B. D., Shull, J. M., & Oegerle, W. R. 2001, ApJ, 561, 573
Sembach, K. R., & Savage, B. D. 1992, ApJS, 83, 147
Sembach, K. R., Tripp, T. M., Savage, B. D., & Richter, P. 2004, ApJS, 155, 351
Shull, J. M., Roberts, D., Giroux, M. L., Penton, S. V., & Fardal, M. A. 1999, AJ, 118, 1450
Shull, J. M., Smith, B. D., & Danforth, C. W. 2011, ArXiv e-prints
Smith, B. D., Hallman, E. J., Shull, J. M., & O'Shea, B. W. 2011, ApJ, 731, 6
Sutherland, R. S., & Dopita, M. A. 1993, ApJS, 88, 253
Thom, C., & Chen, H.-W. 2008, ApJS, 179, 37
Tripp, T. M., Giroux, M. L., Stocke, J. T., Tumlinson, J., & Oegerle, W. R. 2001, ApJ, 563, 724
Tripp, T. M., Sembach, K. R., Bowen, D. V., Savage, B. D., Jenkins, E. B., Lehner, N., & Richter, P. 2008, ApJS, 177, 39
Tumlinson, J., Shull, J. M., Giroux, M. L., & Stocke, J. T. 2005, ApJ, 620, 95
Weymann, R. J., Vogel, S. N., Veilleux, S., & Epps, H. W. 2001, ApJ, 561, 559
Williger, G. M., Heap, S. R., Weymann, R. J., Davé, R., Ellingson, E., Carswell, R. F., Tripp, T. M., & Jenkins, E. B. 2006, ApJ, 636, 631

Summary of IGM Baryon Fraction Results

Ion	$\Omega_{\rm ion}$ (10^{-8}) (> 10 mÅ)	$\Omega_{\rm ion}$ (10^{-8}) (> 30 mÅ)	$\Omega_{\rm IGM}^{\rm (ion)}/\Omega_b$ [a] (> 10 mÅ)	$\Omega_{\rm IGM}^{\rm (ion)}/\Omega_b$ [a] (> 30 mÅ)
O VI	48.22 ± 3.77	40.33 ± 4.28	0.086 ± 0.007	0.072 ± 0.008
N V	4.19 ± 2.25	2.42 ± 2.85	0.059 ± 0.032	0.034 ± 0.040
C IV	20.11 ± 2.01	19.83 ± 2.06	0.067 ± 0.007	0.066 ± 0.007
C III	10.83 ± 1.38	8.75 ± 1.46	0.013 ± 0.002	0.010 ± 0.002
Si IV	11.07 ± 1.57	10.78 ± 1.78	0.099 ± 0.014	0.097 ± 0.016
Si III	17.53 ± 3.21	17.26 ± 4.27	0.061 ± 0.011	0.060 ± 0.015
Fe III	40.16 ± 14.31	29.48 ± 16.93	0.082 ± 0.029	0.060 ± 0.035

[a] Scaled by $f_{\rm ion}$, Z, and H_0; $\Omega_b = 0.0455 \pm 0.0028$ (Komatsu et al. 2011). See text for details.